Journal of Alloys and Compounds 723 (2017) 252–257

Contents lists available at ScienceDirect

Journal of Alloys and Compounds

journal homepage: http://www.elsevier.com/locate/jalcom

Review

Synthesis, structure and anti-oxidation properties of FeNi nanoparticles coated by BN (hexagonal)

Binbin Xu, Yujin Li, Qilei Sun, Wei Zhang, Yujie Zhang, Fanbin Meng*

School of Materials Science and Engineering, Hebei University of Technology, Guangrong Road No. 29, Hongqiao District, Tianjin, 300130, PR China

ARTICLE INFO

Article history:
Received 30 November 2016
Received in revised form
24 May 2017
Accepted 4 June 2017
Available online 24 June 2017

Keywords:
FeNi NPs
Coated
FeNi/BN
Anti-oxidation
Magnetic

ABSTRACT

BN-coated FeNi nanoparticles (i.e., FeNi/BN) has been prepared via liquid phase reduction process followed by high temperature calcination. TEM and SEM images confirm the nano-dimensional structure with core/shell structure, with FeNi NPs as core and BN layers as shell. The anti-oxidation performance of the coated and uncoated powders were investigated from room temperature to 900 °C by TGA and DTA, thermal analysis data revealed that the FeNi NPs are oxidized at 220 °C in the air, while the FeNi/BN samples are stable below 570 °C. This results from the fact that the enhancement of the thermal stability by the BN shell. In addition, the BN layers limit the growth of FeNi NPs, resulting in the lower saturation magnetization and higher coercivity, compared with pure FeNi NPs.

Contents

1. Introduction 252
2. Experimental procedures 253
 2.1. Materials 253
 2.2. Preparation of FeNi Nps 253
 2.3. Preparation of FeNi/BN 253
 2.4. Characterization 253
3. Results and discussion 253
 3.1. Crystal structure and functional groups analysis 253
 3.2. Morphology and particle size analysis 254
 3.3. Magnetic and thermal stability properties analysis 255
4. Conclusion 256
 Acknowledgement 256
 References 256

1. Introduction

Traditional soft magnetic materials of FeNi NPs are different from Fe and Ni NPs with high permeability, surface magnetism and low energy loss have been widely used in electromagnetic wave absorber, high density magnetic recording materials, high effective catalyst and diagnostics agents [1–6]. Unfortunately, oxidation and wear of the metal surfaces are fatal flaws when the size of the alloy is decreased to nanometer level, and the oxidation would actually worsen the magnetic properties of alloy [7].

One way to solve these drawbacks is to coat soft-magnetic metallic nanoparticles with an inorganic coating to build the core/shell nanostructure, such as silicon dioxide [8], graphite [9] and boron nitride [10]. The coating structure not only transforms

* Corresponding author.
E-mail address: mengfanbin4037@163.com (F. Meng).

http://dx.doi.org/10.1016/j.jallcom.2017.06.042
0925-8388/

the magnetic properties of the alloy, but also improves the anti-oxidation of the alloy. Hexagonal boron nitride (h-BN) has received considerable attention due to its high thermal stability, electrical conductivity, low dielectric constant and mechanical strength [11,12], widely used in gaseous uptake, protective coatings, advanced ceramic composites and catalyst support [13–19]. Therefore, the h-BN layers are ideal shells because they can protect metal nanoparticles effectively against oxidation and limit the growth of the alloy.

Several process, including magetron, ion-beam co-sputtering [20] and spraying methods [21] have been developed to prepare BN coated nanoparticles. However, these methods still exit all sorts of drawbacks such as complicated working procedure and difficulty in microstructure control. It has been urgent affairs to produce a large number of nanocapsules with good property.

The purpose of the present work is threefold. The first was to develop a new and simple method for producing the FeNi/BN samples, therefore, the mixture of FeNi alloy precursors and H_3BO_3 powders were selected. The second purpose was to investigate the microstructure of FeNi NPs and FeNi/BN samples by means of X-ray powder diffraction, Transmission electron microscopy and Field emission scanning electron microcopy. The last was to compare the oxidation temperature of pure FeNi NPs and FeNi/BN, these characterization data will provide us with guideline for researching the BN-coated nanostructure materials.

2. Experimental procedures

2.1. Materials

Hexagonal boron nitride (h-BN) powders were synthesized via a simple high-temperature approach (900 °C). Iron nitrate hexahydrate, nickel nitrate hexahydrate, sodium borohydride, polyvinylpyrrolidone and ethanol were used in the experiment are analytically pure grade. Deionized water (DI water) is produced by a water purification machine.

2.2. Preparation of FeNi Nps

Firstly, 1.16 g nickel nitrate hexahydrate and 0.404 g iron nitrate hexahydrate were dissolved into a beaker with 60 ml alcohol for mixing. Then, adding 1.6 g PVP-K30 and 0.6 g sodium borohydride under stirring until dissolved, the black precipitate were obtained and washed to neutral by deionized water and ethanol for several times before dried at 60 °C for 6 h in a vacuum. The dried mixture (i.e., FeNi alloy precursors) was annealed with flowing ammonia at 900 °C for 2 h to obtain FeNi NPs.

2.3. Preparation of FeNi/BN

The FeNi alloy precursors and H_3BO_3 powders with molar ratio of 4:1 were well mixed by triturator. Then, the mixture powders were placed in an alumina tube mounted in a tube furnace and heated up to a temperature of 900 °C with flowing ammonia for 2 h, and naturally cooled (6 h) to room temperature to give a black precipitate.

2.4. Characterization

The phases formed in the FeNi NPs and FeNi/BN were characterized by X-ray diffraction (XRD, Japan, Rigaku smartlab) having Cu-Kα radiation (λ = 0.15405 Å) at a scanning rate of 8° per second in the 2θ range from 10° to 90°. Chemical bonding and groups were determined by fourier transform infrared spectroscopy (FTIR, Vector 22, Germany) between 500 and 4000 cm^{-1}. The morphology and microstructure of samples were investigated by transmission electron microscopy (TEM, Tecnai G2 F20, Netherlands) and field emission scanning electron microscopy (SEM, FEI Company, USA) with an energy dispersive analysis of X-rays (EDAX). The oxidation mechanism of samples were measured by thermal gravimetric analysis (TGA) and scanning differential thermal analysis (SDTA) during heating up from room temperature to 900 °C with 5 °C/min in air. The magnetic properties of FeNi NPs and FeNi/BN were evaluated by vibrating sample magnetometer (VSM, 7404, America) run under 20000 Oe field.

3. Results and discussion

3.1. Crystal structure and functional groups analysis

Fig. 1 illustrates the XRD patterns of the (a) FeNi NPs, (b) h-BN powders and (c) FeNi/BN. The characterization diffraction peaks at 44.30°, 51.56°and 75.90° are assigned to the (111), (200) and (220) crystallographic plants of FeNi NPs (Fig. 1(a)). As exhibited in Fig. 1(b), the peaks located at 25.86°, 41.78° and 76.32° matched well the (002), (100) and (110) reflections of the crystalline plants of h-BN [22–24]. After BN coated on the surface of FeNi NPs, as Fig. 1(c) shown, it is obviously observed that the characterization peaks of FeNi/BN are in good accordance with the bragg diffractions of FeNi NPs and h-BN powders, indicating that FeNi NPs can be relatively well combined with the h-BN. In addition, no peaks of metal hydroxides and metal oxides could be found throughout out the reaction and the good crystallinity of the samples were shown by strong peak intensity and narrow peak width, demonstrating that the purity of products were high and without oxidated, due to the better reducibility of ammonia gas and the protection of boron nitride layers.

Fig. 2 shows the FT-IR spectrum of (a) h-BN and (b) FeNi/BN. As is shown in Fig. 2(b), FeNi/BN exhibits three main distinct peaks of B–N–B, B–N and B–NH_2/B–OH bending at 785 cm^{-1}, 1383 cm^{-1} and 3451 cm^{-1}, respectively. The high frequency peaked at 3451 cm^{-1} is a typical –OH stretching vibration from surface atmosphere species [25]. Both of three peaks can be found in two samples, predicating the existing of BN phase in the sample. It should be noted that, the relative peak intensity of B-N-B and B-N bending vibration are decreased significantly compared with h-BN powders. It could be attributed to the presence of BN coating. Moreover, the h-BN presents additional peaks at 1080 cm^{-1} and

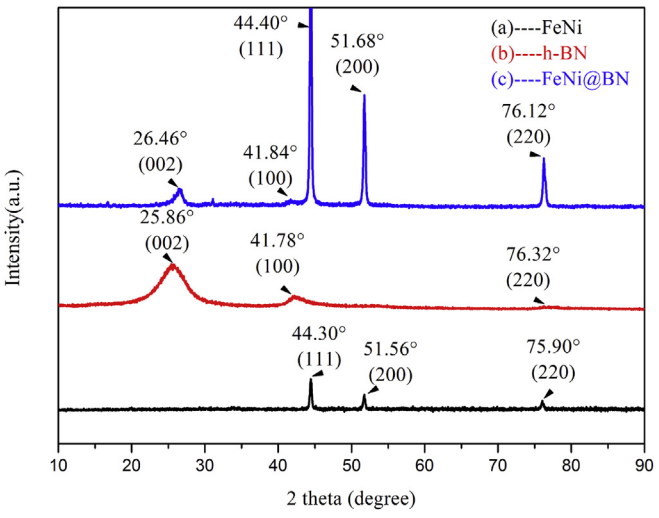

Fig. 1. XRD patterns of (a) FeNi NPs, (b) h-BN powders and (c) FeNi/BN.

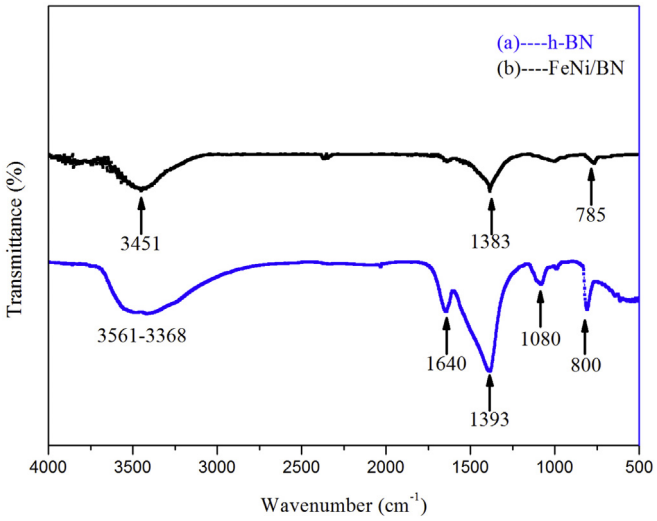

Fig. 2. FT-IR spectrum of (a) h-BN powders and (b) FeNi/BN.

1650 cm^{-1}, which belong to C–O and C=O stretching vibration [26–28]. The characterization data have confirmed that the impurity of C and O in FeNi/BN would be greatly reduced with the addition of FeNi alloy precursors as well as different synthesis routes. The formation of FeNi/BN and h-BN are expressed as follow:

$$FeNi + 2H_3BO_3 + 2NH_3 \rightarrow 2BN + FeNi + 6H_2O$$

$$2H_3BO_3 + C_3N_6H_6 \rightarrow C_3N_6H_6 \cdot 2H_3BO_3 \rightarrow 2BN + 3H_2O + 2CO + 3NH_3 + N_2$$

3.2. Morphology and particle size analysis

In order to investigate the detailed microstructure of the FeNi NPs and FeNi/BN, the samples were further characterized clearly by TEM and SEM techniques. The low-magnification TEM images in Fig. 3(a and b) exhibits the overall morphology of the FeNi/BN and have bight and black areas, indicating that the FeNi NPs with diameter size of 20–200 nm are dispersed in h-BN fibre. The sample displayed good uniformity and a smooth morphology. High-resolution TEM image (Fig. 3(c)) displays the FeNi NPs were completely encapsulated by h-BN shell. The interlayer distance of the BN coating with well crystallized is calculated to be 0.338 nm, corresponding to the interplanar distance of 0.33 nm in bulk hexagonal or rhombohedral BN (002). The inter-lattice distance of the core is 0.208 nm is slightly larger than the interplanar distance 0.204 nm of fcc Fe, matching well the plane of FeNi NPs (111), which confirms that the core is FeNi alloy.

Fig. 4 clearly showed a typical low magnification SEM images and energy dispersive analysis of X-rays (EDAX) of samples. From Fig. 4(a and b), it is obviously seen that the FeNi NPs are formed in a very well regular crystalline shape. These grains are spherical or ellipsoid with a diameter of 100–600 nm, although there were some aggregated particles. The SEM images of FeNi/BN were described in Fig. 4(c and d), compared with original alloys, the FeNi NPs are in the size of 20–250 nm trapped into boron nitride coating, exhibited by the bright contrast. In addition, alloys

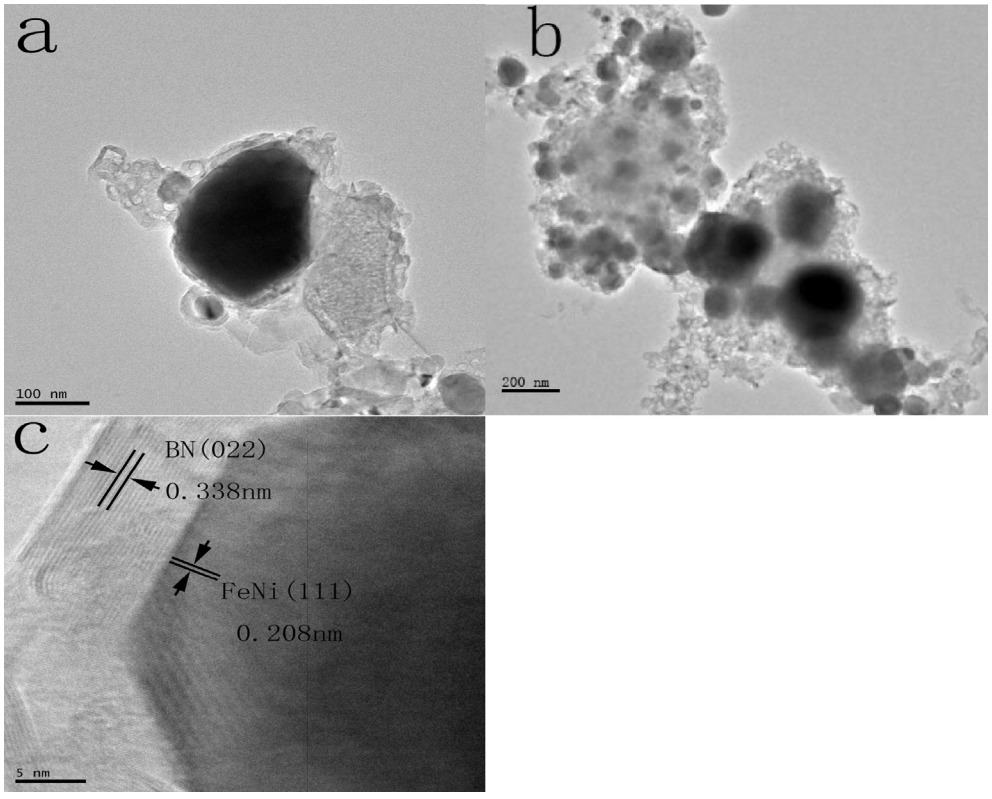

Fig. 3. TEM images of (a, b) FeNi/BN. HRTEM image of (c) FeNi/BN.

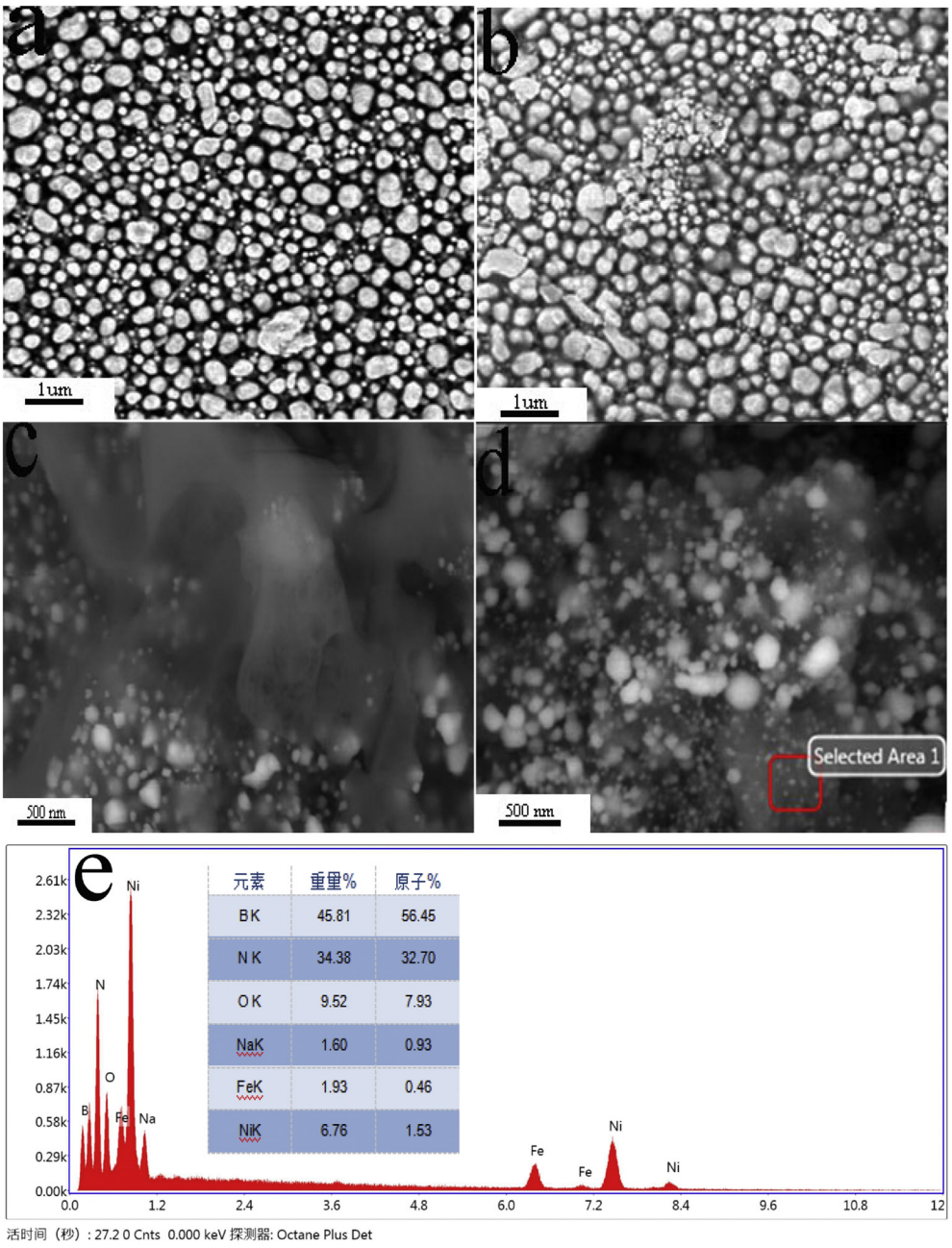

Fig. 4. SEM images of (a, b) FeNi NPs and (c, d) FeNi/BN. EDAX spectrum of (e) FeNi/BN.

essentially retain the spherical morphology, it's remarkable that the h-BN shell has restricted the growth of the alloy and no conglobation phenomenon of grains were observed.

The EDAX spectra of the FeNi/BN was shown in Fig. 4(e). N, B, Fe, Ni, Na and O elements could be found in "Selected Area 1". It is worth noting that the molar ratio of Fe and Ni elements is about 1:4, corresponding to the $Fe(NO_3)_3 \cdot 9H_2O$ and $Ni(NO_3)_2 \cdot 6H_2O$ chemicals in liquid phase reduction solution. The impurity of Na and O elements are little derived from sodium borohydride and ethanol, respectively. The characterization data have confirmed that a great deal of FeNi NPs are sank into the h-BN layers and the growth of FeNi NPs coated with h-BN layers were formed synchronously [6] when annealed the mixture of FeNi alloy precursors and H_3BO_3 powders with flowing ammonia at 900 °C for 2 h.

3.3. Magnetic and thermal stability properties analysis

The hysteresis loops of FeNi NPs and FeNi/BN were measured by vibrating sample magnetometer (VSM) at room temperature. Fig. 5 presents that the FeNi/BN has ferromagnetic behaviors and its saturation magnetization Ms is 76.42 emu/g, which is smaller than the figure 96.19 emu/g of FeNi NPs. Its coercivity Hr is 127.33 Oe, while the FeNi NPs is 99.57 Oe. The decrease of saturation magnetization is attributed to the existence of BN coating. In addition, the diminish grain size of the alloy will reduce the intrinsic magnetic properties (saturation magnetization and magnetic anisotropy) of the material, and smaller magnetic particles in the powders are superparamagnetic also reduce the saturation magnetization. The coercivity of magnetic powder particles is obviously dependent on its size. In the process of magnetization

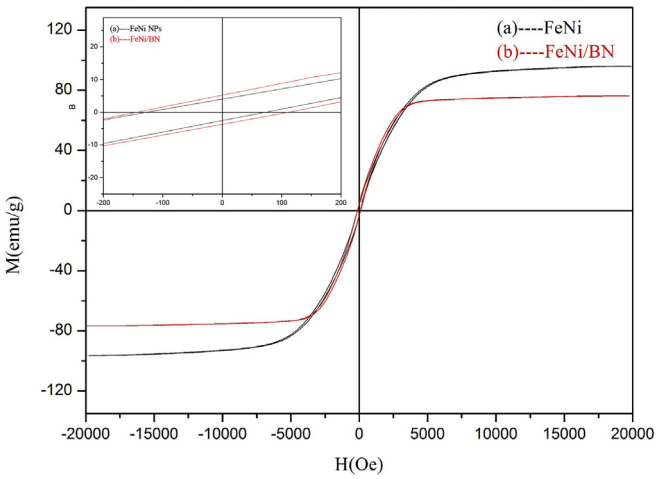

Fig. 5. The hysteresis loop of (a) FeNi NPs and (b) FeNi/BN.

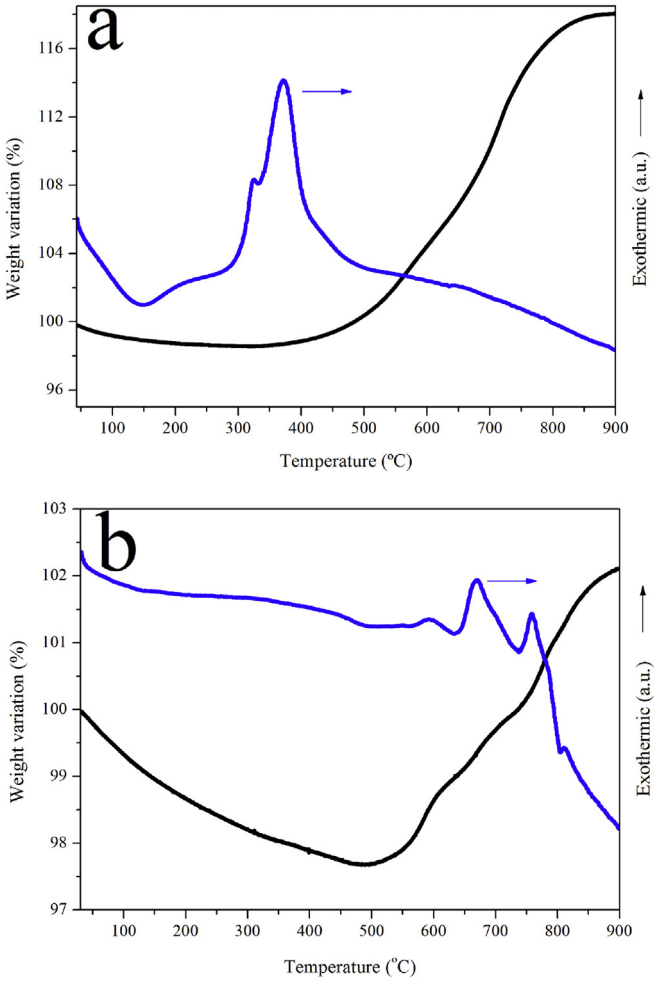

Fig. 6. TGA and SDTA curves of (a) FeNi NPs and (b) FeNi/BN.

reversal, the size of FeNi NPs is smaller and the spin direction of particles is not parallel will improve its static magnetic energy, resulting in higher coercivity. In addition, the coercivity of multi-domain particles is mainly related to the movement of domain walls. The existence of a large number of grain boundaries and coating defects on the FeNi/BN surfaces can reduce the domain walls energy at a certain location. Effectively pinning the movement of the domain wall or setting a energy barriers in front of the domain wall will inhibit domain wall further move through defects. Domain wall pinning more serious, the higher the coercivity [29].

The oxidation behavior of FeNi NPs and FeNi/BN was investigated by TGA and SDTA in a flowing-air stream from room temperature to 900 °C with a heating speed of 5 °C/min. As described in Fig. 6(a), the curves of FeNi NPs presented three different peaks and weight change. The endothermic peak at about 140 °C with a corresponding weight loss is less than 2%, which is a physical evaporates of water molecules in the FeNi NPs surfaces. In addition, the oxidation of FeNi NPs takes place at about 220 °C, accompanying two exothermic peaks over 300 °C, which speculated that the samples had high-speed and serious oxidation reactions from FeNi to monoxides, with the increase of temperature, the monoxides were further oxidated to trioxides as the gradient of TGA curve was sharp. When the temperature of heat treatment is higher than 800 °C, the TGA curve remains substantially stationary, which means that the oxidation reaction is substantially complete.

The curves of FeNi/BN in the range from 500 °C to 900 °C reveal a gradual weight gain, associated with a series of exothermic peaks (as shown in Fig. 6(b)). As we can see that boron nitride encapsulated FeNi NPs are stable in air below 570 °C. The first two exothermic peak at about 600 °C, implying that the cores have undergone two steps of oxidation form FeNi alloy to trioxides, which is almost consistent with pure FeNi NPs. It is worth noting that the coated alloy has increased its anti-oxidant capacity by more than 2 times. It is generally known that the oxidation temperature of BN fibre is above 800 °C in air. However, the FeNi/BN has a large quantity of coating and vacancies defects are active sites for O_2 attack [30], and thus the oxidation temperature of BN shell and BN fibre are 735 °C and 805 °C, associated with two exothermic peaks at over 750 °C. Thermal analysis data indicated that the BN coating can effectively improve anti-oxidation properties of FeNi NPs.

4. Conclusion

The FeNi/BN has been prepared by annealing the mixture of FeNi alloy precursors and H_3BO_3 powders with flowing ammonia at 900 °C for 2 h. SEM and TEM exhibited that the FeNi/BN with BN layers as shell and FeNi NPs as core. The BN layers exist a lot of coatings defects and limit the growth of FeNi NPs, which induce higher Hr and lower Ms. The TGA and SDTA investigates that BN layers can help FeNi/BN nanoparticles to be stable securely below 570 °C in the air, while FeNi nanoparticles are oxidized at about 220 °C. Therefore, the h-BN coated FeNi NPs with excellent magnetic properties and good stability in air, which play a significant synergistic effect in improving comprehensive properties in many fields, such as environmental, energy and industry.

Acknowledgement

This work is supported by the National Natural Science Foundation of China (Grant No. 51371075).

References

[1] A.K. Gupta, M. Gupta, Synthesis and surface engineering of iron oxide nanoparticles for biomedical applications, J. Biomater. 26 (2005) 3995–4021.
[2] A.K. Gupta, M. Gupta, Cytotoxicity suppression and cellular uptake enhancement of surface modified magnetic nanoparticles, J. Biomater. 26 (2005) 1565–1573.
[3] S.L. Wang, Studies of electroless plating of Ni–Fe–P alloys and the influences of some deposition parameters on the properties of the deposits, J. Surf. Coat.

Technol. 186 (2004) 372–376.
[4] V.M. Nadutov, A.I. Ustinov, S.A. Demchenkov, Y.O. Svystunov, V.S. Skorodzievski, Structure and properties of nanostructured vacuum-deposited foils of invar Fe–(35–38 wt%)Ni alloys, J. Mater. Sci. Technol. 31 (2015) 1079–1086.
[5] M.E. Mchenry, D.E. Laughlin, Nano-scale materials development for future magnetic application, Acta Mater. 48 (2000) 223–238.
[6] B. Kim, M.A. Carignano, S.L. Tripp, A. Wei, Cluster size analysis of two-dimensional order in colloidal gold nanoparticle arrays, Langmuir 20 (2004) 9360–9365.
[7] D.L. Fan, J. Feng, S.Y. Zhang, X.M. Lv, T.Y. Gao, Synthesis structure and magnetic properties of Ni and Co nanoparticles encapsulated by few-layer h-BN, J. Alloy Compd. 689 (2016) 153–160.
[8] C.H. Yu, N. Caiulo, C.C.H. Lo, K. Tam, S.C. Tsang, Synthesis and fabrication of a thin film containing silica encapsulated face-centered tetragonal FePt nanoparticles, Adv. Mater. 18 (2006) 2312–2314.
[9] Z.L. Liu, F. He, F. Gao, B.J. Ren, Y. Huang, Fabrication and electromagnetic properties of novel FeNi alloy-coated flake graphite prepared by electroless plating, J. Alloy Compd. 656 (2016) 51–57.
[10] Y. Bando, K. Ogawa, D. Golbrg, Insulating 'nanocables': invar Fe–Ni alloy nanorods inside BN nanotubes, J. Chem. Phys. Lett. 26 (2001) 349–351.
[11] R.T. Paine, C.K. Narula, Synthetic routes to boron nitride, Chem. Rev. 90 (1990) 73–91.
[12] C.Y. Zhi, Y. Bando, C.C. Tang, H. Kuwahara, D. Golberg, Large-scale fabrication of boron nitride nanosheets and their utilization in polymeric composites with improved thermal and mechanical properties, Adv. Mater. 21 (2009), 2889–3289.
[13] X.L. Meng, N. Lun, Y.X. Xin, H.L. Zhu, F.D. Han, L.W. Yin, R.H. Fan, Y.J. Bai, Simple synthesis of mesoporous boron nitride with strong cathodoluminescence emission, J. Solid State Chem. 184 (2011) 859–862.
[14] J.A. Perdigon-Melon, A. Auroux, C. Guimon, B.J. Bonnetot, Micrometric BN powders used as catalyst support: influence of the precursor on the properties of the BN ceramic, J. Solid State Chem. 177 (2004) 609–615.
[15] I.P. Borovinskaya, V.A. Bunin, A.G. Merzhanov, Self-propagating high-temperature synthesis of high-porous boron nitride, Mendeleev Commun. 7 (1997) 47–48.
[16] C.C. Tang, Y. Bando, X.X. Ding, S.R. Qi, D. Golberg, Catalyzed collapse and enhanced hydrogen storage of BN nanotubes, J. Am. Chem. Soc. 124 (2002) 14550–14551.
[17] G. Lian, X. Zhang, S.J. Zhang, D. Liu, D.L. Cui, Q.L. Wang, Controlled fabrication of ultrathin-shell BN hollow spheres with excellent performance in hydrogen storage and wastewater treatment, Energ Environ. Sci. 5 (2012) 7072–7080.
[18] C.Y. Zhi, Y. Bando, T.S. Terao, C. Tang, D. Golberg, Dielectric and thermal properties of epoxy/boron nitride nanotube composites, Pure Appl. Chem. 82 (2010) 2175–2183.
[19] C.Y. Zhi, N. Hanagata, Y. Bando, D. Golberg, Dispersible shortened boron nitride nanotubes with improved molecule loading capacity, Chem. Asian 6 (2011) 2530–2535.
[20] T. Hayashi, S. Hirono, M. Tomita, S. Umemura, Magnetic thin films of cobalt nanocrystals encapsulated in graphite-like carbon, Nature 381 (1996) 772–774.
[21] S.C. Tsang, V. Caps, I. Paraskevas, D. Chadwick, D. Thompset, Magnetically separable, carbon-supported nanocatalysts for the manufacture of fine chemicals, Angew. Chem. Int. Ed. 116 (2004) 5763–5767.
[22] F. Cao, Y. Ding, L. Chen, C.R. Zhang, Improvement of crystallization of borazine-derived boron nitride using small amounts of Fe or Ni nanoparticles, Nanoscale 5 (2013) 10000–10006.
[23] T. Oku, T. Kusunose, K. Niihara, K. Suganuma, Chemical synthesis of silver nanoparticles encapsulated in boron nitride nanocages, J. Mater Chem. 10 (2000) 255–257.
[24] H.S. Lim, J.W. Oh, S.Y. Kim, M.J. Yoo, S.D. Park, W.S. Lee, Anisotropically alignable magnetic boron nitride platelets decorated with iron oxide nanoparticles, Chem. Mater. 25 (2013) 3315–3319.
[25] D.J. Lee, B. Lee, K.H. Park, H.J. Ryu, S. Jeon, S.H. Hong, Scalable exfoliation process for highly soluble boron nitride nanoplatelets by hydroxide-assisted ball milling, Nano Lett. 15 (2015) 1238–1244.
[26] M.I. Baraton, L. Boulanger, M. Cauchetier, V. Lorenzelli, M. Luec, T. Merle, P. Quintard, Y.H. Zhou, J. Eur. Ceram. Soc. 13 (1994) 371–378.
[27] D.L. Fan, J. Feng, J. Liu, T.Y. Gao, Z.X. Ye, M. Chen, X.M. Lv, Hexagonal boron nitride nanosheets exfoliated by sodium hypochlorite ball mill and their potential application in catalysis, Ceram. Int. 42 (2016) 7155–7163.
[28] C.C. Tang, Y. Bando, Y. Huang, C.Y. Zhi, D. Golberg, Synthetic routes and formation mechanisms of spherical boron nitride nanoparticles, Adv. Funct. Mater. 18 (2008) 3653–3661.
[29] R. Fischer, H. Kronmüller, The role of the exchange interaction in nanocrystalline isotropic $Nd_2Fe_{14}B$–magnets, J. Magn. Magn. Mater. 191 (1999) 225–233.
[30] X.G. Liu, Z.Q. Ou, D.Y. Geng, Z. Han, J.J. Jiang, W. Liu, Z.D. Zhang, Influence of a graphite shell on the thermal and electromagnetic characteristics of FeNi nanoparticles, J. Carbon 48 (2010) 891–897.